JOURNAL OF GUIDANCE, CONTROL, AND DYNAMICS
Vol. 30, No. 6, November–December 2007

Engineering Notes

ENGINEERING NOTES are short manuscripts describing new developments or important results of a preliminary nature. These Notes should not exceed 2500 words (where a figure or table counts as 200 words). Following informal review by the Editors, they may be published within a few months of the date of receipt. Style requirements are the same as for regular contributions (see inside back cover).

Relative Semimajor Axis Uncertainty in High Earth Orbits

Christopher Lane* and Penina Axelrad†
University of Colorado, Boulder, Colorado 80309-0431

DOI: 10.2514/1.31881

I. Introduction

SEVERAL proposed missions have identified satellite formation flying in high Earth orbit (HEO) as an enabling technology for increasing the science return while decreasing total mission risk [1,2]. Precision formation flying in HEO requires accurate estimation of the semimajor axis difference between the vehicles for state prediction, formation control, and formation maneuver planning [3–5]. This Note derives the complete linearized mapping relating relative position and velocity error to semimajor axis uncertainty for HEO formations.

The majority of relative navigation filters estimate the state of the secondary vehicle with respect to the primary in Cartesian position and velocity coordinates [6–13]. The uncertainty in the semimajor axis is found by rotating the estimated position and velocity covariance into orbital element space. Carpenter and Schiesser [3] presented the complete linearized relationship between absolute position and velocity uncertainty and semimajor axis error; however, the form of their result is not particularly intuitive. Carpenter and Alfriend [4] used a similar method to develop a simplified expression for the semimajor axis uncertainty that assumes the radial position and velocity and intrack velocity are the primary contributions. However, this assumption is not justified for eccentric orbits. The generalized relationship between relative position and velocity uncertainty and semimajor axis uncertainty is derived here explicitly. The resulting equation shows that the semimajor axis error is dependent on all of the coplanar position and velocity uncertainties in highly eccentric orbits.

The coordinate frames that form the foundation of this research are described in Sec. II. The generalized relationship between position and velocity error and semimajor axis uncertainty is derived in Sec. III, and the conclusions are summarized in Sec. IV.

II. Coordinate Frames

A. Relative Keplerian Element Frame

Consider the motion of two vehicles in nearby eccentric orbits. The trajectory of the primary vehicle, termed the chief, is described by the classical set of Keplerian elements

$$\alpha_* = \begin{bmatrix} a_* & e_* & i_* & \Omega_* & \omega_* & M_* \end{bmatrix}^T$$

where a is the semimajor axis, e is the eccentricity, i is the inclination, Ω is the right ascension of the ascending node, ω is the argument of perigee, and M is the mean anomaly. Note the subscript $*$ is used to designate properties of the chief. The trajectory of the secondary vehicle, termed the deputy, is similarly defined by the set of Keplerian elements

$$\alpha = \begin{bmatrix} a & e & i & \Omega & \omega & M \end{bmatrix}^T$$

Thus, the relative state of the deputy with respect to the chief in the relative Keplerian element (RKE) frame is

$$\delta\alpha = \alpha - \alpha_* = \begin{bmatrix} \delta a & \delta e & \delta i & \delta\Omega & \delta\omega & \delta M \end{bmatrix}^T$$

where it is well known that in certain orbital geometries some Keplerian elements are ill defined [14,15]. In particular, if $e = 0$, then ω is undefined and if $i = 0$, then Ω is undefined. Alternate sets of orbital elements that avoid these singularities can be implemented if the orbit of interest is problematic [14,15]. However, only inclined, eccentric orbits are considered here, and thus, the traditional set of Keplerian elements a, e, i, Ω, ω, and M are used for clarity.

B. Curvilinear Radial, Intrack, and Cross-Track Frame

The curvilinear radial, intrack, and cross-track (RIC) frame is shown in Fig. 1. It is a noninertial frame centered at the chief and defined by the following basis vectors and their time derivatives [15,16]:

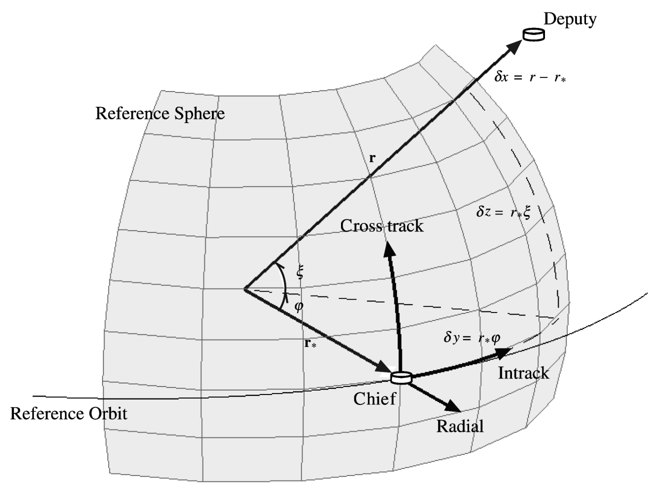

Fig. 1 The radial, intrack, and cross-track (RIC) frame.

Received 30 April 2007; revision received 29 May 2007; accepted for publication 29 May 2007.

*Graduate Student, Aerospace Engineering Sciences, 431 UCB; christopher.lane@colorado.edu. Student Member AIAA.
†Professor and Associate Chair, Aerospace Engineering Sciences, 431 UCB; penina.axelrad@colorado.edu. Associate Fellow AIAA.

$$
\begin{aligned}
&\mathbf{R}_* \equiv \frac{\mathbf{r}_*}{r_*}, \qquad \mathbf{C}_* \equiv \frac{\mathbf{r}_* \times \mathbf{v}_*}{|\mathbf{r}_* \times \mathbf{v}_*|}, \qquad \mathbf{I}_* \equiv \mathbf{C}_* \times \mathbf{R}_* \\
&\frac{\mathrm{d}\mathbf{R}_*}{\mathrm{d}t} = \frac{\mathbf{v}_*}{r_*} - \frac{\mathbf{r}_* \cdot \mathbf{v}_*}{r_*^3}\mathbf{r}_* \\
&\frac{\mathrm{d}\mathbf{C}_*}{\mathrm{d}t} = \frac{\mathbf{r}_* \times \mathbf{a}_*}{|\mathbf{r}_* \times \mathbf{v}_*|} - \frac{(\mathbf{r}_* \times \mathbf{v}_*)\cdot(\mathbf{r}_* \times \mathbf{a}_*)}{|\mathbf{r}_* \times \mathbf{v}_*|^3}(\mathbf{r}_* \times \mathbf{v}_*) \\
&\frac{\mathrm{d}\mathbf{I}_*}{\mathrm{d}t} = \frac{\mathrm{d}\mathbf{C}_*}{\mathrm{d}t} \times \mathbf{R}_* + \mathbf{C}_* \times \frac{\mathrm{d}\mathbf{R}_*}{\mathrm{d}t}
\end{aligned} \tag{1}
$$

where $\mathbf{r}$, $\mathbf{v}$, and $\mathbf{a}$ are the Earth-centered-inertial (ECI) position, velocity, and acceleration vectors, respectively, of the vehicle and $r = |\mathbf{r}|$. In Fig. 1, a reference sphere of radius r_* is defined, tangent to the $\mathbf{I} - \mathbf{C}$ plane at the chief. The radial component of the relative position δx is the difference between r and r_*; the curvilinear intrack and cross-track relative positions, δy and δz, are measured along the surface of the sphere as indicated in the figure. Mathematically, they are defined as follows [15–18]. The radial component δx is given by

$$
\delta x = r - r_*, \qquad \delta\dot{x} = \frac{\mathbf{r}\cdot\mathbf{v}}{r} - \frac{\mathbf{r}_*\cdot\mathbf{v}_*}{r_*} \tag{2}
$$

The intrack component δy is given by

$$
\delta y = r_*\varphi, \qquad \delta\dot{y} = \frac{\mathbf{r}_*\cdot\mathbf{v}_*}{r_*}\varphi + r_*\dot{\varphi} \tag{3}
$$

where

$$
\tan(\varphi) = \frac{\mathbf{R}\cdot\mathbf{I}_*}{\mathbf{R}\cdot\mathbf{R}_*}
$$

and

$$
\begin{aligned}
\dot{\varphi} = \frac{1}{1+\tan^2(\varphi)}\Bigg[&\frac{1}{\mathbf{R}\cdot\mathbf{R}_*}\left(\mathbf{R}\cdot\frac{\mathrm{d}\mathbf{I}_*}{\mathrm{d}t} + \frac{\mathrm{d}\mathbf{R}}{\mathrm{d}t}\cdot\mathbf{I}_*\right) \\
&- \frac{\mathbf{R}\cdot\mathbf{I}_*}{(\mathbf{R}\cdot\mathbf{R}_*)^2}\left(\mathbf{R}\cdot\frac{\mathrm{d}\mathbf{R}_*}{\mathrm{d}t} + \frac{\mathrm{d}\mathbf{R}}{\mathrm{d}t}\cdot\mathbf{R}_*\right)\Bigg]
\end{aligned}
$$

The cross-track component δz is given by

$$
\delta z = r_*\xi, \qquad \delta\dot{z} = \frac{\mathbf{r}_*\cdot\mathbf{v}_*}{r_*}\xi + r_*\dot{\xi} \tag{4}
$$

where

$$
\sin(\xi) = \mathbf{R}\cdot\mathbf{C}_*
$$

and

$$
\dot{\xi} = \frac{1}{\cos(\xi)}\left(\mathbf{R}\cdot\frac{\mathrm{d}\mathbf{C}_*}{\mathrm{d}t} + \frac{\mathrm{d}\mathbf{R}}{\mathrm{d}t}\cdot\mathbf{C}_*\right)
$$

Thus, the relative state of the deputy with respect to the chief in the curvilinear RIC frame is

$$
\delta\mathbf{X} = \begin{bmatrix} \delta x & \delta y & \delta z & \delta\dot{x} & \delta\dot{y} & \delta\dot{z} \end{bmatrix}^T
$$

III. Covariance Transformation

Let $\delta\hat{\mathbf{X}}$ denote the linear, unbiased, minimum variance estimate of the true state $\delta\mathbf{X}$ and $P_{\delta\mathbf{X}}$ the associated estimation error covariance matrix [19],

$$
P_{\delta\mathbf{X}} \equiv E[(\delta\hat{\mathbf{X}} - \delta\mathbf{X})(\delta\hat{\mathbf{X}} - \delta\mathbf{X})^T]
= \begin{bmatrix}
\sigma_{\delta x}^2 & \rho_{\delta x\delta y}\sigma_{\delta x}\sigma_{\delta y} & \cdots & \rho_{\delta x\delta\dot{z}}\sigma_{\delta x}\sigma_{\delta\dot{z}} \\
\rho_{\delta x\delta y}\sigma_{\delta x}\sigma_{\delta y} & \sigma_{\delta y}^2 & \cdots & \rho_{\delta y\delta\dot{z}}\sigma_{\delta y}\sigma_{\delta\dot{z}} \\
\vdots & & \ddots & \vdots \\
\rho_{\delta x\delta\dot{z}}\sigma_{\delta x}\sigma_{\delta\dot{z}} & \rho_{\delta y\delta\dot{z}}\sigma_{\delta y}\sigma_{\delta\dot{z}} & \cdots & \sigma_{\delta\dot{z}}^2
\end{bmatrix}
$$

where the diagonal elements represent the variance of the estimation error and the off-diagonal terms are a measure of the cross correlation between the estimated uncertainties. The covariance matrix in the RKE frame, $P_{\delta\alpha}$, can be similarly defined as

$$
P_{\delta\alpha} \equiv E[(\delta\hat{\alpha} - \delta\alpha)(\delta\hat{\alpha} - \delta\alpha)^T]
= \begin{bmatrix}
\sigma_{\delta a}^2 & \rho_{\delta a\delta e}\sigma_{\delta a}\sigma_{\delta e} & \cdots & \rho_{\delta a\delta M}\sigma_{\delta a}\sigma_{\delta M} \\
\rho_{\delta a\delta e}\sigma_{\delta a}\sigma_{\delta e} & \sigma_{\delta e}^2 & \cdots & \rho_{\delta e\delta M}\sigma_{\delta e}\sigma_{\delta M} \\
\vdots & & \ddots & \vdots \\
\rho_{\delta a\delta M}\sigma_{\delta a}\sigma_{\delta M} & \rho_{\delta e\delta M}\sigma_{\delta e}\sigma_{\delta M} & \cdots & \sigma_{\delta M}^2
\end{bmatrix}
$$

where $\delta\hat{\alpha}$ is the linear, unbiased, minimum variance estimate of $\delta\alpha$.

Relative filters typically provide an estimate of $\delta\mathbf{X}$ and $P_{\delta\mathbf{X}}$. The uncertainty in the relative semimajor axis can be obtained by rotating $P_{\delta\mathbf{X}}$ into the RKE frame using the linear transformation

$$
[P_{\delta\alpha}]_{\delta\mathbf{X}} = \Gamma_*^{-1} P_{\delta\mathbf{X}} \Gamma_*^{-1^T} \tag{5}
$$

where $[P_{\delta\alpha}]_{\delta\mathbf{X}}$ is the linear approximation of $P_{\delta\alpha}$ given $P_{\delta\mathbf{X}}$, and Γ_*^{-1} is the inverse of the mapping matrix relating $\delta\mathbf{X}$ to $\delta\alpha$,

$$
\delta\mathbf{X} \approx \Gamma_*\delta\alpha
$$

A brief development of Γ_* and Γ_*^{-1} is presented in the Appendix; the complete derivation is found in Lane and Axelrad [16]. Note similar equations relating $\delta\mathbf{X}$ and $\delta\alpha$ are found in [17,18,20–22].

Evaluating Eq. (5) using the results from the Appendix yields the following expression for the relative semimajor axis uncertainty as a function of the elements of $P_{\delta\mathbf{X}}$:

$$
\begin{aligned}
[\sigma_{\delta a}^2]_{\delta\mathbf{X}}
&\approx \frac{4[1+e_*\cos(\upsilon_*)]^2}{1-e_*^2}\left\{\frac{[2+e_*\cos(\upsilon_*)]^2[1+e_*\cos(\upsilon_*)]^2}{(1-e_*^2)^3}\sigma_{\delta x}^2\right. \\
&\left. + 2\frac{[2+e_*\cos(\upsilon_*)][1+e_*\cos(\upsilon_*)]}{n_*(1-e_*^2)^{3/2}}\rho_{\delta x\delta\dot{y}}\sigma_{\delta x}\sigma_{\delta\dot{y}} + \frac{1}{n_*^2}\sigma_{\delta\dot{y}}^2\right\} \\
&- \frac{8[1+e_*\cos(\upsilon_*)]e_*\sin(\upsilon_*)}{1-e_*^2}\left\{\frac{[2+e_*\cos(\upsilon_*)][1+e_*\cos(\upsilon_*)]^3}{(1-e_*^2)^3}\right. \\
&\times \rho_{\delta x\delta y}\sigma_{\delta x}\sigma_{\delta y} - \frac{[2+e_*\cos(\upsilon_*)][1+e_*\cos(\upsilon_*)]}{n_*(1-e_*^2)^{3/2}}\rho_{\delta x\delta\dot{x}}\sigma_{\delta x}\sigma_{\delta\dot{x}} \\
&\left. + \frac{[1+e_*\cos(\upsilon_*)]^2}{n_*(1-e_*^2)^{3/2}}\rho_{\delta y\delta\dot{y}}\sigma_{\delta y}\sigma_{\delta\dot{y}} - \frac{1}{n_*^2}\rho_{\delta\dot{x}\delta\dot{y}}\sigma_{\delta\dot{x}}\sigma_{\delta\dot{y}}\right\} \\
&+ \frac{4e_*^2\sin^2(\upsilon_*)}{1-e_*^2}\left\{\frac{[1+e_*\cos(\upsilon_*)]^4}{(1-e_*^2)^3}\sigma_{\delta y}^2\right. \\
&\left. - 2\frac{[1+e_*\cos(\upsilon_*)]^2}{n_*(1-e_*^2)^{3/2}}\rho_{\delta y\delta\dot{x}}\sigma_{\delta y}\sigma_{\delta\dot{x}} + \frac{1}{n_*^2}\sigma_{\delta\dot{x}}^2\right\}
\end{aligned} \tag{6}
$$

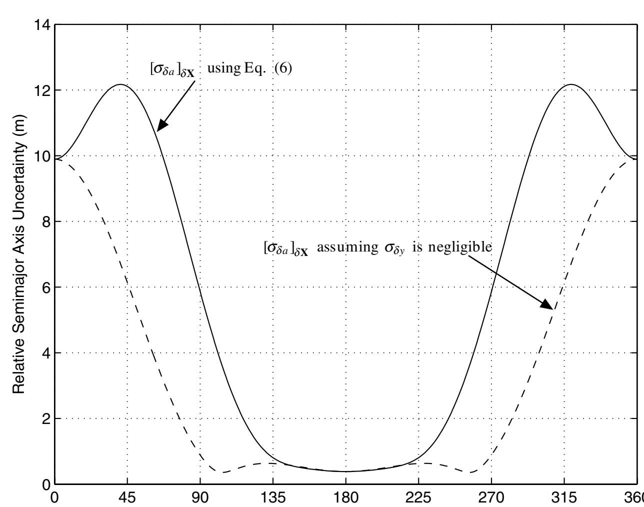

Fig. 2 Comparison of relative semimajor axis uncertainty for $a_* = 42,096$ km, $e_* = 0.8$, $\sigma_{\delta x} = 0.1$ m, $\sigma_{\delta y} = 0.5$ m, $\sigma_{\delta\dot{x}} = 0.01$ mm/s, and $\sigma_{\delta\dot{y}} = 0.05$ mm/s.

where n_* is the mean motion of the reference orbit. The accuracy of Eq. (6) depends on the validity of the mapping matrix Γ_*^{-1}, which is a function of the separation between the vehicles in both position *and* velocity.

In near-circular orbits, $e \approx 0$ and Eq. (6) reduces to

$$[\sigma_{\delta a}^2]_{\delta\mathbf{X}} \approx 4\left[4\sigma_{\delta x}^2 + \frac{4}{n_*}\rho_{\delta x\delta\dot{y}}\sigma_{\delta x}\sigma_{\delta\dot{y}} + \frac{1}{n_*^2}\sigma_{\delta\dot{y}}^2\right] \tag{7}$$

This is identical to the result obtained in [3–5]. From Eq. (7), it is easy to show that $\sigma_{\delta a} = 0$ when $\rho_{\delta x\delta\dot{y}} = -1$ and $\sigma_{\delta\dot{y}}/\sigma_{\delta x} = 2n$. Thus, if the uncertainty in the radial position and intrack velocity are highly correlated and properly balanced, a perfect estimate of δa can be achieved in near-circular orbits. A similar set of correlation and balance requirements can be derived for eccentric orbits using Eq. (6). However, as noted by Mitchell et al. [5], control over $\sigma_{\delta x}$, $\sigma_{\delta y}$, $\sigma_{\delta\dot{x}}$, $\sigma_{\delta\dot{y}}$, and the associated cross correlations is necessary to achieve the desired constraints, and there is no method for tuning these elements independently in a Kalman filter.

In [4], the primary focus is on the uncertainty in the relative semimajor axis derived assuming the principal components are the radial position and velocity and intrack velocity errors. However, in Eq. (6), it is clear $[\sigma_{\delta a}]_{\delta\mathbf{X}}$ is a function of all of the coplanar uncertainties in highly eccentric orbits. This is illustrated for a simple example in Fig. 2 for $a_* = 42,096$ km, $e_* = 0.8$, $\sigma_{\delta x} = 0.1$ m, $\sigma_{\delta y} = 0.5$ m, $\sigma_{\delta\dot{x}} = 0.01$ mm/s, and $\sigma_{\delta\dot{y}} = 0.05$ mm/s. Note that $\rho_{\delta x\delta\dot{y}} = -1$ and $\rho_{\delta y\delta\dot{x}} = 1$ in Fig. 2; the cross correlations $\rho_{\delta x\delta y}$, $\rho_{\delta x\delta\dot{x}}$, $\rho_{\delta y\delta\dot{y}}$, and $\rho_{\delta\dot{x}\delta\dot{y}}$ are assumed to be negligible. In Fig. 2, ignoring the contribution of $\sigma_{\delta y}$ leads to dramatically underestimating the relative semimajor axis uncertainty for most of the orbit.

IV. Conclusions

This Note has derived the complete linearized relationship between relative position and velocity and relative semimajor axis error for highly eccentric orbits. This approach was shown to be a direct generalization of the circular orbit solution and account for errors in all of the coplanar uncertainties. The results indicate that previous assumptions (of semimajor axis error being solely dependent on radial position and velocity and intrack velocity error) lead to underestimating the relative semimajor axis uncertainty for significant portions of the orbit. This has important implications for formation flying in HEO where precise semimajor axis knowledge is essential to mission operations. It is possible to derive the complete nonlinear mapping relating position and velocity to the semimajor axis error, but this degree of fidelity is not required for most applications.

Appendix: Derivation of Mapping Matrix Γ_*

The derivation of the mapping matrix Γ_* begins with the expressions relating ECI position and velocity to Keplerian elements [14]

$$\mathbf{r} = r\begin{bmatrix}\cos(\Omega)\cos(\theta) - \sin(\Omega)\cos(i)\sin(\theta)\\ \sin(\Omega)\cos(\theta) + \cos(\Omega)\cos(i)\sin(\theta)\\ \sin(i)\sin(\theta)\end{bmatrix}, \qquad \mathbf{v} = \sqrt{\frac{\mu}{a(1-e^2)}}\begin{bmatrix}-\cos(\Omega)[\sin(\theta) + e\sin(\omega)] + \sin(\Omega)\cos(i)[\cos(\theta) + e\cos(\omega)]\\ -\sin(\Omega)[\sin(\theta) + e\sin(\omega)] - \cos(\Omega)\cos(i)[\cos(\theta) + e\cos(\omega)]\\ \sin(i)[\cos(\theta) + e\cos(\omega)]\end{bmatrix} \tag{A1}$$

where $\theta = \omega + \upsilon$ and

$$r = \frac{a(1-e^2)}{1 + e\cos(\upsilon)}$$

Expanding the definition of $\delta\mathbf{X}$ in Eqs. (2–4) around α_* using Eq. (A1) gives Γ_*,

$$\Gamma_* = \begin{bmatrix}\gamma_*\\ \gamma'_*\end{bmatrix}$$

where

$$\gamma_* = \begin{bmatrix}\frac{r_*}{a_*} & -a_*\cos(\upsilon_*) & 0 & 0 & 0 & \frac{a_* e_* \sin(\upsilon_*)}{\sqrt{1-e_*^2}}\\ 0 & \left(a_* + \frac{r_*}{1-e_*^2}\right)\sin(\upsilon_*) & 0 & r_*\cos(i_*) & r_* & \frac{a_*^2}{r_*}\sqrt{1-e_*^2}\\ 0 & 0 & r_*\sin(\theta_*) & -r_*\sin(i_*)\cos(\theta_*) & 0 & 0\end{bmatrix}$$

$$\gamma'_* = \dot{r}_*\begin{bmatrix}-\frac{1}{2a_*} & 0 & 0 & 0 & 0 & 0\\ 0 & \frac{\sin(\upsilon_*)}{1-e_*^2} & 0 & \cos(i_*) & 1 & -\left(\frac{a_*}{r_*}\right)^2\sqrt{1-e_*^2}\\ 0 & 0 & \sin(\theta_*) & -\sin(i_*)\cos(\theta_*) & 0 & 0\end{bmatrix}$$
$$+ \dot{\upsilon}_*\begin{bmatrix}0 & a_*\sin(\upsilon_*) & 0 & 0 & 0 & \frac{a_* e_* \cos(\upsilon_*)}{\sqrt{1-e_*^2}}\\ -\frac{3r_*}{2a_*} & \left(a_* + \frac{r_*}{1-e_*^2}\right)\cos(\upsilon_*) & 0 & 0 & 0 & 0\\ 0 & 0 & r_*\cos(\theta_*) & r_*\sin(i_*)\sin(\theta_*) & 0 & 0\end{bmatrix}$$

and

$$\dot{r}_* = \frac{a_* e_* n_* \sin(\upsilon_*)}{\sqrt{1-e_*^2}}, \qquad \dot{\upsilon}_* = \left(\frac{a_*}{r_*}\right)^2 n_*\sqrt{1-e_*^2}$$

Inverting Γ_* yields

$$\Gamma_*^{-1} = [\gamma_*^{-1} \mid \gamma_*'^{-1}]$$

where

$$\gamma_*^{-1} = \begin{bmatrix} [4+2e_*\cos(\upsilon_*)]\left(\frac{a_*}{r_*}\right)^2 & -2e_*\sin(\upsilon_*)\left(\frac{a_*}{r_*}\right)^2 & 0 \\ \frac{e_*\cos^2(\upsilon_*)+3\cos(\upsilon_*)+2e_*}{r_*} & \frac{[e_*\cos^2(\upsilon_*)+2\cos(\upsilon_*)+e_*]e_*\sin(\upsilon_*)}{a_*(1-e_*^2)} & 0 \\ 0 & 0 & \frac{e_*\sin(\omega_*)+\sin(\theta_*)}{a_*(1-e_*^2)} \\ 0 & 0 & -\frac{e_*\cos(\omega_*)+\cos(\theta_*)}{a_*(1-e_*^2)\sin(i_*)} \\ \frac{\{[2+e_*\cos(\upsilon_*)]^2-1\}\sin(\upsilon_*)}{a_*e_*(1-e_*^2)} & \frac{e_*\cos^3(\upsilon_*)+2\cos^2(\upsilon_*)-1}{a_*(1-e_*^2)} & \frac{[e_*\cos(\omega_*)+\cos(\theta_*)]\cos(i_*)}{a_*(1-e_*^2)\sin(i_*)} \\ -\frac{\{[2+e_*\cos(\upsilon_*)]^2-(1-e_*^2)\}\sin(\upsilon_*)}{a_*e_*\sqrt{1-e_*^2}} & \frac{[2+e_*\cos(\upsilon_*)]\sin^2(\upsilon_*)}{a_*\sqrt{1-e_*^2}} & 0 \end{bmatrix}$$

$$\gamma_*^{\prime -1} = \begin{bmatrix} \frac{2e_*\sin(\upsilon_*)}{n_*\sqrt{1-e_*^2}} & \frac{2[1+e_*\cos(\upsilon_*)]}{n_*\sqrt{1-e_*^2}} & 0 \\ \frac{\sin(\upsilon_*)\sqrt{1-e_*^2}}{a_*n_*} & \frac{[e_*\cos^2(\upsilon_*)+2\cos(\upsilon_*)+e_*]\sqrt{1-e_*^2}}{a_*n_*[1+e_*\cos(\upsilon_*)]} & 0 \\ 0 & 0 & \frac{\cos(\theta_*)\sqrt{1-e_*^2}}{a_*n_*[1+e_*\cos(\upsilon_*)]} \\ 0 & 0 & \frac{\sin(\theta_*)\sqrt{1-e_*^2}}{a_*n_*[1+e_*\cos(\upsilon_*)]\sin(i_*)} \\ -\frac{\cos(\upsilon_*)\sqrt{1-e_*^2}}{a_*e_*n_*} & \frac{[2+e_*\cos(\upsilon_*)]\sin(\upsilon_*)\sqrt{1-e_*^2}}{a_*e_*n_*[1+e_*\cos(\upsilon_*)]} & \frac{\sin(\theta_*)\sqrt{1-e_*^2}\cos(i_*)}{a_*n_*[1+e_*\cos(\upsilon_*)]\sin(i_*)} \\ \frac{[e_*\cos^2(\upsilon_*)+\cos(\upsilon_*)-2e_*](1-e_*^2)}{a_*e_*n_*[1+e_*\cos(\upsilon_*)]} & -\frac{[2+e_*\cos(\upsilon_*)]\sin(\upsilon_*)(1-e_*^2)}{a_*e_*n_*[1+e_*\cos(\upsilon_*)]} & 0 \end{bmatrix}$$

Acknowledgments

This work was funded under Cooperative Agreement NCC5-721 through the NASA Goddard Space Flight Center Formation Flying NASA Research Announcement. Any opinions, findings and conclusions or recommendations expressed in this material are those of the authors and do not necessarily reflect the views of the National Aeronautics and Space Administration.

References

[1] Leitner, J., Bauer, F., Folta, D., Moreau, M., Carpenter, R., and How, J., "Formation Flight in Space," *GPS World*, Feb. 2002, pp. 22–31, http://www.gpsworld.com/gpsworld/article/articleDetail.jsp?id=9518 [retrieved 26 July 2007].

[2] Fisher, R. R., and Weiler, E. J., "Magnetospheric Multiscale Mission (MMS)," Jan. 2003, NASA Announcement of OpportunityAO-03-OSS-01, http://research.hq.nasa.gov/code_s/dynamic.cfm?op_fy=2003[26 July 2007].

[3] Carpenter, J. R., and Schiesser, E., "Semimajor Axis Knowledge and GPS Orbit Determination," *Journal of the Institude of Navigation*, Vol. 48, No. 1, 2001, pp. 47–68.

[4] Carpenter, J. R., and Alfriend, K. T., "Navigation Accuracy Guidelines for Orbital Formation Flying," *Journal of the Astronautical Sciences*, Vol. 53, No. 2, 2005, pp. 207–219.

[5] Mitchell, M., Breger, L., and How, J. P., "Effects of Navigation Filter Properties on Formation Flying Control," AIAA Paper 2004-5024, Aug. 2004.

[6] Kawano, I., Mokuno, M., Kasai, T., and Suzuki, T., "First Autnomous Rendezvous Using Relative GPS Navigation by ETS-VII," *Journal of the Institute of Navigation*, Vol. 48, No. 1, 2001, pp. 393–400.

[7] Park, C.-W., "Precise Relative Navigation Using Augmented CDGPS," Ph.D. Thesis, Stanford University, Stanford, CA, June 2001.

[8] Ebinuma, T., "Precision Spacecraft Rendezvous Using Global Positioning System: An Integrated Hardware Approach," Ph.D. Thesis, University of Texas, Austin, TX, Aug. 2001.

[9] Long, A., Kelbel, D., Lee, T., Leung, D., Carpenter, J. R., and Gramling, C., "Relative Navigation for Formation-Flying Satellites," *1st International Symposium on Formation Flying Mission and Technology*, Computer Sciences Corp., Lanham, MD, Oct. 2002.

[10] Kelbel, D., Lee, T., Long, A., Carpenter, R., and Gramling, C., "Relative Navigation Algorithms for Phase 1 of MMS formation," *Flight Mechanics Symposium*, NASA Goddard Space Flight Center, Greenbelt, MD, 2003.

[11] Busse, F. D., "Precise Formation-State Estimation in Low Earth Orbit Using Carrier Differential GPS," Ph.D. Thesis, Stanford University, Stanford, CA, March 2003.

[12] Leung, S., and Montenbruck, O., "Real-Time Navigation of Formation-Flying Space Using Global-Positioning-System Measurements," *Journal of Guidance, Control, and Dynamics*, Vol. 28, No. 2, 2005, pp. 226–235.

[13] Mohiuddin, S., and Psiaki, M. L., "Satellite Relative Navigation Using Carrier-Phase Differential GPS with Integer Ambiguities," AIAA Paper 2005-6054, Aug. 2005.

[14] Battin, R., *An Introduction to the Mathematics and Methods of Astrodynamics*, AIAA Education Series, AIAA, New York, 1987.

[15] Vallado, D., *Fundamentals of Astrodynamics and Applications*, 2nd ed., Microcosm Press, El Segundo, CA, 2001.

[16] Lane, C., and Axelrad, P., "Analysis of Relative Navigation in High Earth Orbits," *Journal of the Astronautical Sciences*, Vol. 55, No. 1, 2007, pp. 291–310.

[17] Broucke, R., "Solution of the Elliptic Rendezvous Problem with the Time as Independent Variable," *Journal of Guidance, Control, and Dynamics*, Vol. 26, No. 4, 2003, pp. 615–621.

[18] Schaub, H., and Junkins, J. L., *Analytical Mechanics of Space Systems*, AIAA Education Series, AIAA, Reston, VA, 2003.

[19] Born, G., Tapley, B., and Schutz, B., *Statistical Orbit Determination*, Elsevier Academic Press, San Francisco, CA, 2004.

[20] Garrison, J. L., Gardner, T. G., and Axelrad, P., "Relative Motion in Highly Elliptical Orbits," *Proceedings of the 5th AAS/AIAA Spaceflight Mechanics Conference*, edited by R. J. Proulx, J. J. F. Liu, P. K. Seidelmann, and S. Alfano, American Astronautical Society, San Diego, CA, Vol. 89, 1995, pp. 1359–1376.

[21] Gim, D. W., and Alfriend, K. T., "State Transition Matrix of Relative Motion for the Perturbed Noncircular Reference Orbit," *Journal of Guidance, Control, and Dynamics*, Vol. 26, No. 6, 2003, pp. 956–971.

[22] Sabol, C., McLaughlin, C. A., and Luu, K. K., "Meet the Cluster Orbits with Perturbations of Keplerian Elements (COWPOKE) Equations," *Advances in the Astronautical Sciences*, Vol. 114, No. 1, 2003, pp. 573–594.